View metadata, citation and similar papers at core.ac.uk

brought to you by CORE

provided by Institutional Research Information System University of Turin

UNIVERSITÀ DEGLI STUDI DI TORINO

This is an author version of the contribution published on:

AQUILANO D., BRUNO M., RUBBO M., MASSARO F. R., PASTERO L.
Low symmetry polymorph of hydroxyapatite. Theoretical equilibrium morphology of the monoclinic Ca5(OH)(PO4)3
CRYSTAL GROWTH & DESIGN (2014) 14
DOI: 10.1021/cg5001478

The definitive version is available at:
http://pubs.acs.org/doi/abs/10.1021/cg5001478

The Low Symmetry Polymorph of Hydroxyapatite. Theoretical Equilibrium Morphology of the Monoclinic $Ca_5(OH)(PO_4)_3$

Dino Aquilano,[1*] Marco Bruno,[1] Marco Rubbo,[1] Francesco Roberto Massaro,[2] Linda Pastero[1]

[1]*Dipartimento di Scienze della Terra, Università degli Studi di Torino, via Valperga Caluso 35, I-10125, Torino, Italy*

[2]*Dipartimento di Geoscienze, Università degli Studi di Padova, Via Gradenigo 6, I-35131, Padova, Italy*

** corresponding author :* dino.aquilano@unito.it

ABSTRACT: The Hartman-Perdok analysis has been carried out on the monoclinic $P2_1/c$ polymorph of Hydroxyapatite (HAp) in order to find the character of the main {hkl} forms and foresee the possible profiles of the related surfaces. Then, the corresponding specific surface energies have been calculated, at 0 K, by *ab initio* quantum-mechanical calculations, and the HAp equilibrium shape has been obtained: a striking pseudo-hexagonal prism comes out from the close similarity of the surface energy of the three pinacoids {001}, {100} and $\{\bar{1}02\}$, all developing around the [010] zone axis which runs parallel to the OH channels of the structure bulk. The most stable form, the pinacoid {010}, truncates the pseudo-hexagonal prism perpendicularly to the OH channels, while the less morphologically important monoclinic prisms {012}, {110} and $\{11\bar{2}\}$ complete the HAp equilibrium shape. Preliminary considerations are exposed about the morphological path: monoclinic polymorph→ twinning →hexagonal polymorph. Finally, a simple kinetic model based on 2D nucleation is proposed to explain the rod shaped morphology of the solution grown monoclinic HAp, as we obtained at room temperature.

1. Introduction

Hydroxyapatite, HAp – $Ca_5(OH)(PO_4)_3$, the primary mineral in hard tissues like bones and teeth, is the most important among the calcium phosphates which, in turn, belong to the largest group of biominerals in vertebrate animals. HAp is characterized by an intriguing polymorphism which is not yet thoroughly understood.

The first determined and also the most frequently encountered HAp polymorph belongs to the *hexagonal system* ($a_0=b_0=9.432$ Å, $c_0=6.881$Å; $\alpha=\beta=90°$, $\gamma=120°$). The space group $P6_3/m$ was assigned to a synthetic specimen investigated by single crystal X-ray diffractometry without

determining the position of hydrogen atoms,[1] while the H position was determined and the same space group confirmed by neutron diffraction, on a natural sample containing 0.28% of Fluorine replacing the OH groups.[2] The $P6_3/m$ setting has been experimentally determined in crystals obtained by hydrothermal synthesis[3-5] and in natural samples[6] where the OH groups are partially replaced by simple ions such as F and Cl. Moreover, it was assumed as a structural model for theoretical studies on growth morphology[7] and surface relaxation,[8] for computing simulation of molecular adsorption on HAp surfaces,[9-12] and for evaluating the formation energies of Na and K replacing the Ca ions of HAp.[13] A lower symmetry hexagonal space group, $P6_3$, has been systematically chosen[14-16] to simulate either the specific surface energies or the interaction of biomolecules with selected crystal surfaces, through *ab initio* quantum-mechanical calculations. The symmetry reduction (from $P6_3/m$ to $P6_3$) is energetically favored and then it was adopted since it brings all OH groups with the same orientation in every structure channel (parallel orientation → ferroelectric ordering); as a matter of fact, the symmetry mirror *m* is not consistent with an ordered alignment of hydroxyl group, for the alternating O and H occupying special positions should be equidistant.

The second HAp polymorph belongs to the *monoclinic system* (a_0= 9.4214, b_0= $2a_0$, c_0= 6.881Å; α=β=90°, γ=120°). In analogy with the observations made by Young and Elliot[17] on pure and stoichiometric Chloro-apatite (ClAp) and on ClAp twins,[18] Elliott confirmed[19] that the space group of the pure synthetic HAp (obtained by heating single ClAp crystals in steam at 1200°C for two weeks[20]) is $P2_1/b$. The screw axes run along the structure channels, while the OH groups, lying on them, point upwards and downwards in alternate nearest neighbors channels, related by the glide plane *b* (antiparallel orientation).

The number of investigations concerning the monoclinic HAp polymorph is not comparable with that on the hexagonal one. This may be due to the difficulty of obtaining the pure monoclinic phase, as shown by Elliott et al.[21] who produced "… a specimen 63% hexagonal and 37% monoclinic…", with the hexagonal to monoclinic ratio varying from specimen to specimen;[22] moreover, twin free monoclinic crystal are quite rare.[23]

Peculiar attention has been deserved to the polymorphic "hexagonal ↔ monoclinic" HAp transition. From X-Ray Powder Diffraction (XRPD) and Differential Scanning Calorimetry (DSC) diagrams it comes out that the high temperature polymorph is hexagonal ($P6_3/m$), while the low temperature phase is monoclinic ($P2_1/b$), the reversible transition taking place at 480.5 K in heating and at 477.5 K in cooling process. Further, the transition enthalpy was found to be quite low: 130 J/mol.[24,25]

Theoretical investigations showed as well that the monoclinic polymorph should be energetically favored than the hexagonal one,[9,26-29] at low temperature. Nevertheless, it is worth remembering that the structural differences between the two polymorphs are very subtle, and then "… the success of their characterization shows the great potential of electron microscopy and electron diffraction techniques for precise phase identification".[30]

Concluding, the relationship between the two polymorphs remains a complex issue:

- the real structure of the hexagonal phase of pure hydroxyapatite is nowadays an open question;
- the twinning geometry of the monoclinic phase is just enounced but nothing is known about both the twin generation and relation between the multiple twin and the hexagonal polymorph;
- experimental growth morphologies are poorly known and, in any case, their interpretation in terms of kinetics and effects of selected impurities remains qualitative;
- literature data do not exist about the surface morphologies of the two polymorphs, that could be a powerful tool to distinguish between symmetries of the crystal bulk;
- information about the theoretical equilibrium and/or growth morphology of the HAp polymorphs are scarce, incomplete and often contradictory; this means that nothing can be predicted about their nucleation frequency.

In this paper we will determine the *ab initio* theoretical equilibrium morphology of the HAp monoclinic polymorph at the temperature of 0K. Vibrational and configurational entropy will not be considered owing to the calculation load, while solvent and impurity effects will be the subject of a successive phase of our research program. The approach we adopted to deal with the surface profiles of the different {*hkl*} forms is that proposed long time ago by Hartman and Perdok (HP hereinafter);[31] this path is somewhat laborious but is supported by the reassuring results obtained for a long time, especially for low symmetry and complex structures. Notably:

i) we will identify the character (flat or stepped) of the most morphological important {*hkl*} forms ;

ii) then, the corresponding slices of d_{hkl} thickness will be considered along with their possible surface profiles fulfilling the stability constraints;

iii) finally, the specific surface energy will be calculated, for each *hkl* surface profile, in order to draw the equilibrium morphology of the single crystal, by applying the Gibbs-Wulff's theorem.[32]

Steps i) $\rightarrow$ iii) are also needed as the preliminary requirement to investigate the crystallography and the genetic aspects of the HAp twins, their original composition planes and, ultimately, to calculate the energy needed for their formation, as we will show in a forthcoming paper.

2. Computational Details

The crystal surfaces were simulated by using the 2D periodic slab model[33] and the *ab initio* CRYSTAL09 code.[34-36] The calculations were performed at the DFT (Density Functional Theory) level: the B3LYP Hamiltonian was adopted,[37-39] which already shown to provide accurate results for structural and dynamical properties of hydroxyapatite. Further computational details (e.g., basis set, thresholds controlling the accuracy of the calculations) are reported in the Supporting Information.

The CRYSTAL09 output files, listing the optimized fractional coordinates and optimized 2D cell parameters of the (001), (100), (10$\bar{2}$), (010), (011) and (012) slabs, are freely available at http://mabruno.weebly.com/download). All of these slabs are charge neutral and retain the centre of inversion, to ensure that the dipole moment perpendicular to the slab is equal to zero.

For our calculations we adopted the optimized conventional cell: a_0=9.3253Å; b_0=6.9503Å; c_0=18.6436Å; β=119.972°, referred to the space group $P2_1/c$ and to 4 unit formulas, i.e.: $Ca_{20}(OH)_4(PO_4)_{12}$. The setting $P2_1/c$ has been preferred to the $P2_1/b$ only because the screw diad axis 2_1 traditionally coincides, in the monoclinic system, with *y* axis.

The specific surface energy γ (erg/cm^2) at T = 0K was calculated by means of the relation:[33]

$$\gamma = \lim_{n\to\infty} E_s(n) = \lim_{n\to\infty} \frac{E(n)_{slab} - nE_{bulk}}{2A} \quad (1)$$

where $E(n)$ and E_{bulk} are the energy of a *n*-layer slab and of the bulk, respectively; A is the area of the primitive unit cell of the surface. $E_s(n)$ is thus the energy (per unit area) required for the formation of the surface from the bulk. When $n \to \infty$, $E_s(n)$ will converge to the surface energy per unit area (γ).

3. Surface profiles obtained from the PBC analysis

3.1. The zone [010]: the forms {100}, {001} and {$\bar{1}$02} and their flat (F) character

3.1.1. The $[010]_A$ PBC and the corresponding surface profiles

The most important periodic bond chain (PBC in the sense of HP[31]) in HAp crystal is the one running along the direction [010]: its period coincides with the modulus of the vector [010] = 6.9503 Å. As one can see in Fig. 1, the [010] PBC develops around the 2_1 screw axis which relates the couples of OH ions having the same orientation; it follows that, in the crystal bulk, one half of these PBCs are polar along the positive direction of the *y* axis while the other half shows opposite polarity.

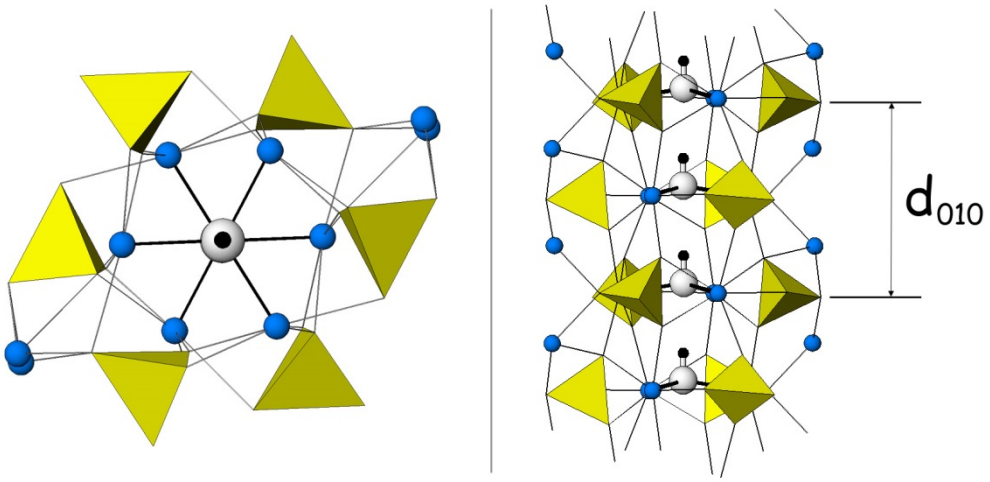

Figure 1. Left: The $[010]_A$ PBC viewed along its development axis $y \equiv 2_1$. Ca–OH bonds are represented by heavy lines, while lighter ones show the Ca–O_{PO_4} bonds. Right: The same PBC viewed perpendicularly to the y axis: its helicoidal aspect is outlined, along with the repeat period d_{010} and the direction of the OH groups. Colors: Ca- blue, $O_{(OH)}$-grey, H-black, (PO_4) tetrahedra-olive.

Over the [010] period, the PBC is stoichiometric, its composition being $Ca_{10}(OH)_2$ $(PO_4)_6$. The two OH ions are bound to six Ca ions which form a pseudo-octahedron as a coordination polyhedron, having two opposite faces crossed by the 2_1 axis; Ca ions are in turn bound to six PO_4 ions forming a second pseudo-octahedron oriented like the preceding one. Finally, the remaining four Ca ions lie external to the PO_4 octahedron and are bound to two PO_4 ions: it is worth remembering that these last Ca ions are two by two symmetry related by the 2_1 axis and lie on a plane containing the 2_1 axis itself. Consequently, the shape of this PBC projected onto the 010 plane is quasi elliptical (Fig.1). Finally, having taken into account that the external Ca ions are in number of twelve, one can find three $[010]_A$ PBCs, according to whether the long axis of the ellipse lie on the $10\bar{1}$ plane, or on the plane $\bar{1}04$ or, finally, on the 102 plane. Accordingly, one can find three PBCs, very similar each other but not symmetry equivalent, that we will call, hereinafter, $[010]_{A1}$, $[010]_{A2}$ and $[010]_{A3}$, respectively.

The importance of these PBCs lies in the fact that they identify the three flat forms (F-forms in the sense of HP) belonging to the [010] zone, i.e.: the pinacoids {100}, {001} and $\{\bar{1}02\}$. As a matter of fact, the F character of these three different forms ensues from the consideration that the PBCs are bound along the directions [001], [100] and [201], respectively. In fact, one can find (Fig. 2) the slices of thickness d_{002}, d_{100} and $d_{\bar{1}02}$ fulfilling the systematic extinction rules (*h0l*, *l=2n*; *00l*, *l=2n*) imposed by the space group $P2_1/c$. Each of these slices contains both the $[010]_A$ PBC and the

[001], [100] and [201] PBCs respectively, and hence the corresponding crystallographic forms are flat (F) and grow layer-by-layer, either by spiral or 2D-nucleation.

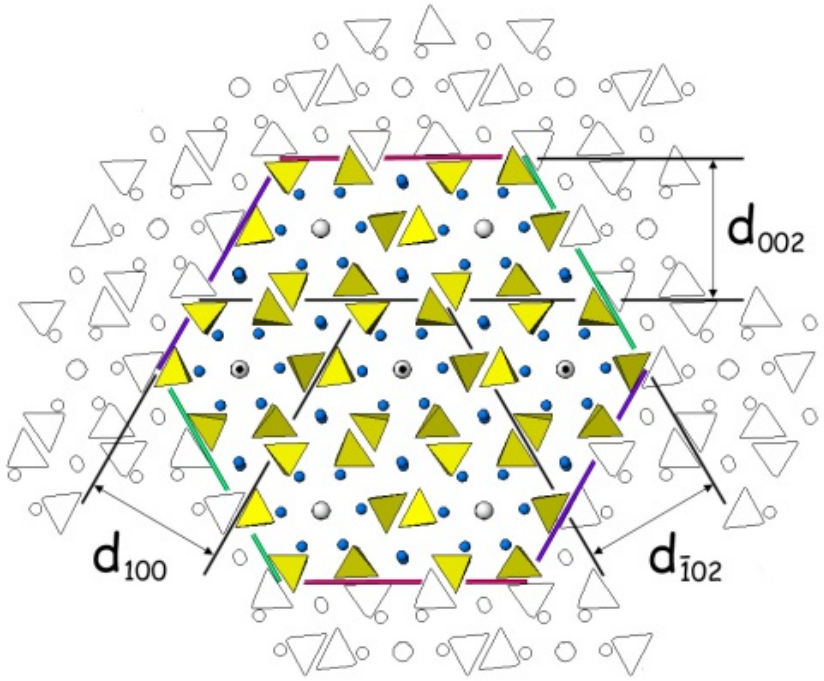

Figure 2. The structure of the monoclinic HAp viewed along the 2_1 axis. The profiles of the forms {100}-blue, {001}-red and {$\bar{1}$02}-green are obtained from the $[010]_A$ PBCs. The thickness of the elementary layers fulfils the extinction rules imposed by the space group $P2_1/c$. It is worth outlining that the OH groups are oriented up-down within the slices d_{100} and $d_{\bar{1}02}$, while they alternate (all up / all down) within the adjacent slices d_{002}.

Looking at Fig. 2, one can see that the surface profiles of the {100}, {001} and {$\bar{1}$02} forms, determined according to HP method, are practically indistinguishable: thus, we could expect that their specific surface energies have close values; their attachment energies, i.e. the energies released (per formula unit) when an elementary slice of thickness d_{hkl} deposits during growth on a pre-existing F face (*hkl*), should also have similar values. Accordingly, both the theoretical equilibrium and growth shapes of the monoclinic HAp crystal could look like a quasi-regular hexagonal prism, in the [010] zone, the more so as the dihedral angle formed between the successive (100) and (001) faces is β = 119.972°, the one between the successive (001) and ($\bar{1}$02) faces is δ = 120.032°, and that between the successive ($\bar{1}$02) and ($\bar{1}$00) faces is ε = 119.995°. Summing up, it is not surprising that the ensemble built by the three monoclinic pinacoids {100}, {001} and {$\bar{1}$02} might be easily confused with the very hexagonal prism of the structurally hexagonal HAp polymorph.

Examining Fig. 2 in deeper detail, one can appreciate that a subtle and not negligible difference exists between the structure of the d_{002} slice and that of both the d_{100} and $d_{\bar{1}02}$ ones: in fact, the d_{100} and $d_{\bar{1}02}$ slices built by the $[010]_A$ PBC are center-symmetric, while the d_{002} slice built by the same $[010]_A$ PBC contains only the screw 2_1 axes parallel to the [010] direction. This implies that a growing HAp crystal can show two terminations of outmost d_{002} slices, according to whether the OH dipoles lying in the middle of the slice are oriented along the positive or negative direction of the *y* axis. On the contrary, the d_{100} and $d_{\bar{1}02}$ slices do not show polarity, neither parallel nor normal to the slice itself, which somewhat could distinguish the values of both surface and attachment energies of {100} and $\{\bar{1}02\}$ with respect to the {001} form.

When summarizing, the most evident features of Fig. 2 are:

- The surface profiles of the three pinacoids {100}, {001} and $\{\bar{1}02\}$ have not to be reconstructed because the corresponding elementary slices do not show dipole moments perpendicular to their surfaces. Further, neither PO_4 tetrahedra nor Ca ions lie on the separation surface between two adjacent slices and hence both ions are not shared between adjacent slices.
- The OH ions in the channels are screened from the mother phase by the outmost layers of each slice populated by PO_4 tetrahedra and by Ca ions not directly bound to the OH in the channels.

3.1.2. The $[010]_B$ PBC and the generation of alternative surface profiles for the forms {100}, {001} and $\{\bar{1}02\}$

In Fig. 3 is illustrated an alternative PBC running along the [010] direction. One can find the two ways of building the $[010]_B$ PBC, which does not contain the OH group in its center, at variance with the $[010]_A$ PBCs.

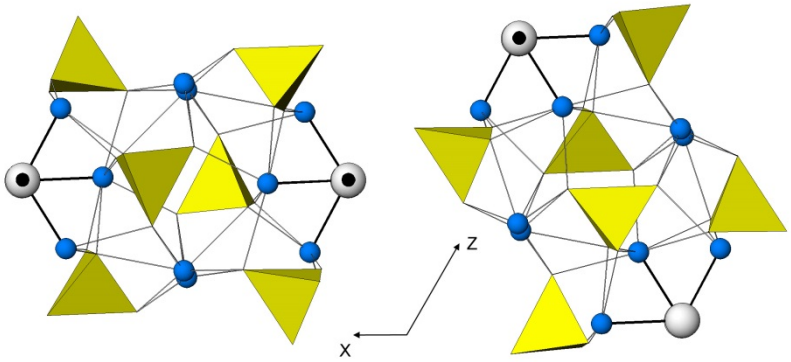

Figure 3. The two ways of building the $[010]_B$ PBC. In both cases the OH groups occupy the extremities of the long axis of the PBC. The symmetry element of the left side-$[010]_B$ PBC is the axis 2_1 // [010], while an inversion center characterizes the right side-$[010]_B$ PBC.

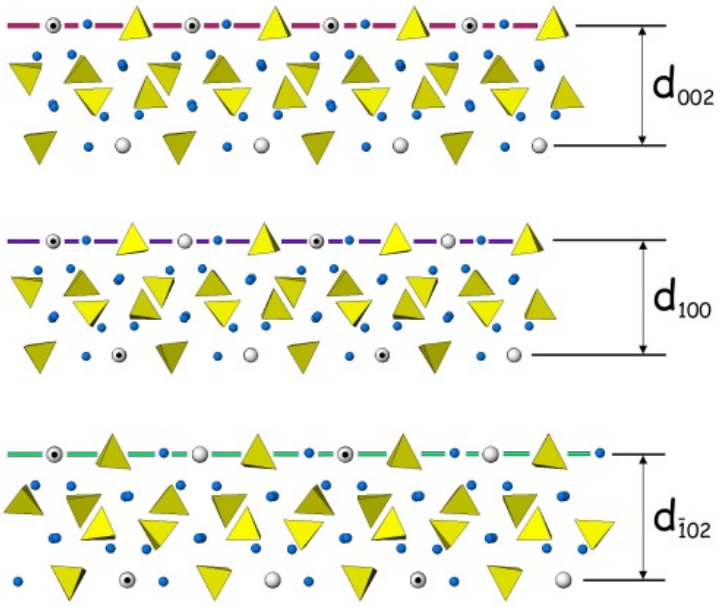

Figure 4. A set of the alternative profiles of the forms {001}, {100} and {$\bar{1}$02}, as one obtains from the PBCs of the type $[010]_B$. Obviously, each of these center-symmetric slices needs to be reconstructed, since each frontier has to be shared between two adjacent equivalent slices. As a consequence, in the outmost layers of each slice only one half of the bulk sites are occupied.

Fig. 4 illustrates one set of the surface terminations that can be obtained from the $[010]_B$ PBC. They deeply differ from those shown in Fig. 2:

- The outmost layers of each slice is populated not only by the PO_4 tetrahedra, but also by Ca ions and OH groups.
- The population of the outmost layers must be reduced by 50%, as it follows from the constraints (of symmetry, charge and stoichiometry) imposed by the frontiers (between adjacent d_{100}, d_{002} and $d_{\bar{1}02}$ slices) passing through the centers of mass of the PO_4, Ca and OH ions.

In relation to the latter observation, it is worth mentioning that the set of surface termination shown in Figs. 3 and 4 represents one of the possible configurations of each outmost layer, compatible with the symmetry centers lying on the mid-plane of each slice. Later on, we will report and discuss the specific relaxed surface energy for this surface multiplicity, having kept in mind that the equilibrium shape of the HAp crystal in the [010] zone will be determined by the minimum surface energy of each of the three {001}, {100} and {$\bar{1}$02} forms.

3.2. The stepped (S) character of the {$10\bar{1}$} form, as follows from the systematic extinction rules

As one can see in the Supporting Information (Fig. S1), a $[010]_{A1}$ PBC can be strongly bound to a $[010]_B$ PBC, along the direction [101]. Accordingly, a slice of thickness $d_{10\bar{1}}$ can be generated with a marked flat character; nevertheless, a slice with this thickness is not allowed by the extinction rule: *h0l,* (*l=2n*) which implies the halving of the slice, i.e. the thickness $d_{20\bar{2}}$. This means that the form $\{10\bar{1}\}$ is stepped, cannot grow layer-by-layer by 2D nucleation, but most likely by uncorrelated direct integration of growth units, implying a high growth rate eventually leading to nil its extension; alternatively, it can grow by spiral mechanism in case the Burger's vector of the dislocation line outcropping on the $\{10\bar{1}\}$ surfaces has a screw component multiple of $\vec{b}$ = ½|[100]| = ½ |[001]| sinβ. We will evaluate in a forthcoming paper the specific surface energy of the $\{10\bar{1}\}$ form in order to determine if it can belong to the equilibrium shape of the [010] zone, although the grooves, the $\{10\bar{1}\}$ profile shows, suggest a relatively high surface energy.

3.3. The {010} form: its F character, surface profiles and the d_{020} slice limited only by Ca ions

The HAp structure is viewed along the [100] direction, Fig. 5. One way to draw a slice of thickness d_{020} is to consider that the adjacent d_{020} slices can be separated by the imaginary planes containing four Ca ions (at *y*=0) and other four (at *y* = ½). These two planes are symmetry related by the glide *c*planes (at *y* = ¼ and *y*= ¾, respectively). Hence, these slices cannot show electrical dipole moment perpendicular to their limiting surfaces and, therefore, they do not need to be reconstructed (Fig. 5, left). Nevertheless, only two out of the Ca ions belonging to a slice frontiers must be considered for each surface profile, because each frontier is shared by two adjacent d_{020} slices. Among the different configurations of the surface Ca layers, we represented in Fig. 5(right) the one in which the surface Ca ions alternate within the 2D surface cell limited by the vectors [100] and [101] ≡ $c_0$senβ.

A second way to draw a slice of thickness d_{020} is illustrated in Fig. S2 (Supporting Information), along with its corresponding surface profile.

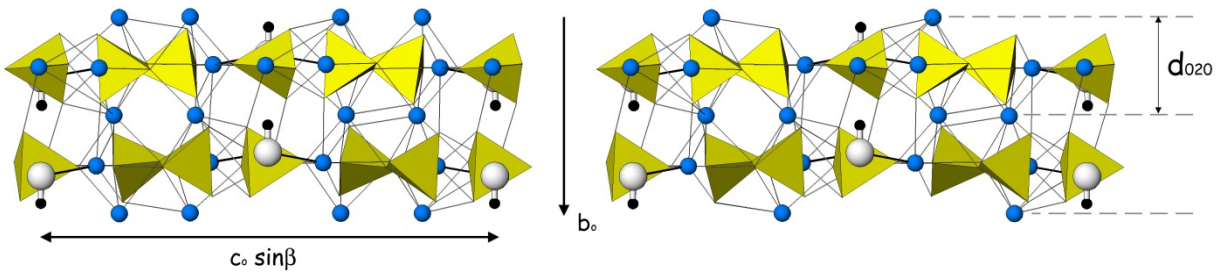

Figure 5. Left: The slice of thickness d_{010}, viewed along the [100] direction. The thickness d_{020} is the one allowed by the extinction rules. Right: One possible configuration of the same slice obtained considering that Ca ions lying at y=0 and y=b_0 belong to the two adjacent d_{010} slices.

3.4. The [100] zone: the prisms {011} and {012}

Projecting the Hap monoclinic structure along the [100] direction is not only useful to determine the surface profiles of the basal {010} pinacoid, but also to investigate if other {0kl} forms can be found in the [100] zone, apart the just described {001} pinacoid.

3.4.1. The prism{011}

The structures of the center-symmetric and stoichiometric $[100]_A$ and $[100]_B$ PBCs are detailed in Fig. S3 (Supporting Information). By alternating them along the $[01\bar{1}]$ direction one determines the slice of thickness d_{011} allowed by the extinction rule of the structure factors for the *hkl* planes: ($k+l = 2n$). This means that the {011} prism can show flat (F) character: its wavy surface profile is drawn in Fig. 6.

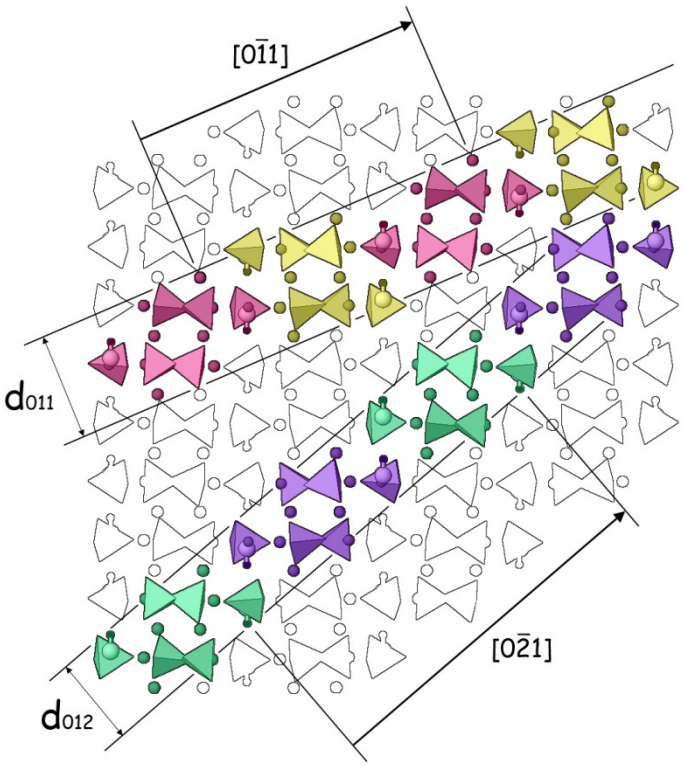

Figure 6. The HAp structure projected along the [100] direction. Top: the slice of thickness d_{011} is allowed by the extinction rules. Bottom: the slice d_{012} forbidden by the extinction rules. Colors identify the $[100]_{A,B,C,D}$ PBCs, as explained in detail in the Supporting Information.

3.4.2. The prism {012}

In Fig. 6 one can also see that a slice of thickness d_{012} is obtained by bounding the $[100]_C$ and $[100]_D$ PBCs along the direction $[0\bar{2}1]$ (Fig. S3). The slice is center-symmetric, its surface profile being terminated by Ca and PO_4 ions along with antiparallel OH groups. There are four equivalent faces: (012), $(01\bar{2})$, $(0\bar{1}2)$ and $(0\bar{1}\bar{2})$ building the monoclinic prism {012}. These faces fulfill all the characteristics in order to be flat (F) faces, but one: due to the size of the [100] PBC, the corresponding thickness of the d_{012} slice is twice that of the d_{024} slice, the only allowed by the extinction rule quoted in section 3.4.1. It follows that the growth mechanisms of the prism {012} can be those illustrated for the $\{10\bar{1}\}$ form.

4. Surface energies and the HAp equilibrium shape

4.1. The surface energy values

The specific surface energy values, calculated for the pinacoids {100}, {001}, $\{10\bar{2}\}$ belonging to the [010] zone, for the basal pinacoid {010}, and for the two prisms {011} and {012}, are reported in Table 1. These values were obtained by optimizing the slabs terminated with the surface profiles originated from the different PBCs we described above.

Table 1. Specific surface energy values (γ) of the F forms of the monoclinic HAp, calculated for the profiles fulfilling the constraints illustrated in columns 2, 3 and 5. When a surface termination exhibits several initial configurations we can find several different optimal configurations and surface energies: the asterisks denote these cases. For each case we report the lowest value of γ.

Form	PBC of reference	Surface termination	γ (erg cm^{-2})	Is the outmost layer shared between adjacent slices?
{010}	$[100]_{A,B,C,D}$	Ca	1041	yes
$\{10\bar{2}\}$	$[010]_B$	PO_4, Ca, OH	1515*	yes
	$[010]_A$	PO_4	1725	no
{001}	$[010]_B$	PO_4, Ca, OH	1546*	yes
	$[010]_A$	PO_4	1712	no

{100}	$[010]_B$	PO_4, Ca, OH	1525*	yes
	$[010]_A$	PO_4	1723	no
{011}	$[100]_{A,B}$	PO_4	1495	yes
{012}	$[100]_{C,D}$	Ca	1637	yes

Table 2. Dispersion of the surface energy values of the {001} form. The value in the 2nd row refers to the unique profile showing only PO_4 tetrahedra in the outmost layer of the slice d_{002} (generated by the $[010]_A$ PBC). Values in the 1st and 3rd row refer to the 8 surface profiles that can be obtained from the dispositions of PO_4, Ca and OH ions in the outmost layer of the alternative d_{002} slice (generated by the $[010]_B$ PBC).

Form	PBC of reference	Surface termination	γ (erg cm^{-2})
	$[010]_B$	PO_4, Ca, OH	1546, 1613, 1666, 1691
{001}	$[010]_A$	PO_4	1712
	$[010]_B$	PO_4, Ca, OH	1738, 1741, 1742, 1793

As an example, all the γ values of the {001} form are reported in Table 2. The surface configuration of the faces (001) generated by the $[010]_A$ PBC is unique, since the outmost layer of each d_{002} slice is not shared between adjacent layers: the corresponding surface energy is 1712 erg cm^{-2}. Conversely, there are eight different configurations of the outermost layer built by the $[010]_B$ PBC, depending on the dispositions of PO_4, Ca and OH ions. The corresponding energy values are distributed in two sets, one half of them being lower and the other one higher than their mean value, 1692 erg cm^{-2}, which is only 1.1% lower than the one corresponding to the unique profile derived from $[010]_A$ PBC. Concerning the dispersion around the mean γ value, it ranges from −8.6 to + 5.97%. Summing up, it is worth remarking that, whatever the d_{002} slice configuration, the dispersion of the surface energy values is fairly moderate.

Let us stress that the {001} form is the most anisotropic in the [010] zone, being the only one (at variance with the {100} and $\{\bar{1}02\}$ forms) in which the OH groups alternate up/down within the successive d_{002} slices (see Fig. 2) and consequently, we expect the surface energy dispersion is even lower for the remaining pinacoids {100} and $\{\bar{1}02\}$.

On the ground of these considerations we preliminary assume that, at equilibrium, the forms belonging to the zones [100], [001] and [201] should have the same properties; accordingly, we

assigned the γ values calculated for the set of forms {001}, {011} and {012} to the two other sets: {100}, {120} and {110}; {10$\bar{2}$}, {12$\bar{2}$} and {112}. Our assumption is even less than an approximation; as a matter of fact, from Fig. 4S and its caption, one can find the strong similarity between the surface profiles of the three sets: {011}, {012}; {120}, {110} and {12$\bar{2}$}, {112}.

4.2. The calculated equilibrium shape (ES) at T=0 K

Taking into account the preliminary conclusions laid out in section 4.1 we built, by the Wulff's theorem,[32] the polyhedron drawn in Fig. 7, using the lowest values of the surface energy for every face. The pseudo-trigonal ES symmetry is striking, as it should come out from the closeness of the γ values of the prisms {100},{001} and {10$\bar{2}$} (1525, 1546 and 1515 erg cm^{-2}, respectively).

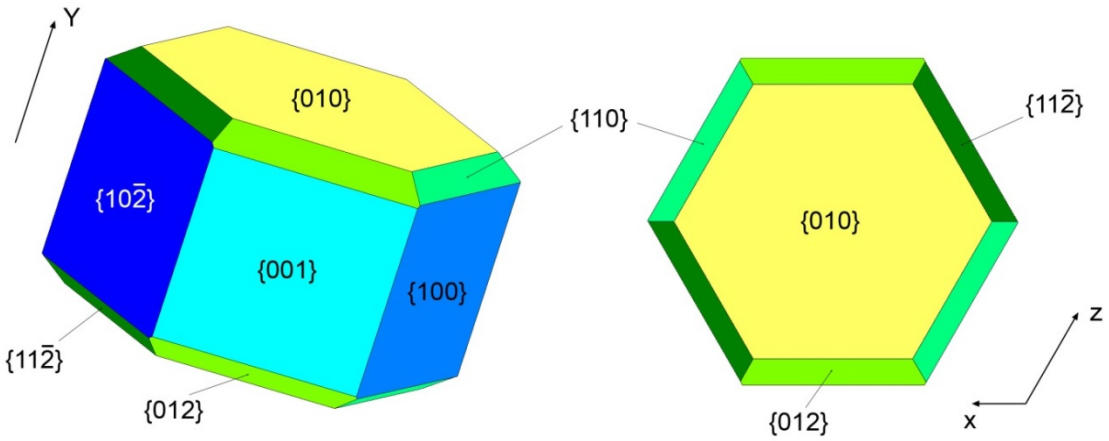

Figure 7. Theoretical equilibrium shape (at 0K) calculated by the Wulff's plot based on the lowest surface energy values reported in Table 1. Faces belonging to the same {hkl} form are equal in color, while color gradations indicate and allow to distinguish crystal forms having very close surface energy values.

It is worth noting that the prisms {011}, {120} and {12$\bar{2}$} do not enter the ES, at T= 0 K, even if their surface energy values are lower than those of the other family of prisms: {012}, {110} and {11$\bar{2}$}. This is only due to the higher slope of the second family with respect to the basal 010 plane. Thermal and configurational entropy contributions could play a not negligible role, so the difference (less that 10%) between the two reference values (1495 and 1637 erg cm^{-2}) could be compensated and hence the situation could be reversed. Moreover, if one does consider the influence of the

solvent adsorption when HAp nucleates and grows from solution, one can whatever expect the appearance of a pseudo-trigonal pyramid in the ES, like that in Fig. 7. Nevertheless, caution should be needed when observing the experimental HAp growth shapes, for only precise measurement of the pseudo-pyramid slope could allow to identify its crystallographic indexes.

5. Discussion and conclusion

a) Applying the Hartman-Perdok analysis to the monoclinic HAp structure, allowed to identify the character and, successively, the most stable surface profiles of the main crystal forms. From *ab initio* calculations of the corresponding specific surface energies, the equilibrium shape at 0K of the crystal (ES) was obtained. This is dominated by the three quasi-equivalent pinacoids {100}, {001}, {$\bar{1}$02}, and by the pinacoid {010}. The three quasi-equivalent prisms, {012}, {110} and {11$\bar{2}$}, clearly show a lower morphological importance. The ES of the monoclinic HAp shows a markedly pseudo-hexagonal 6/m symmetry, our results being in good agreement with those, qualitatively obtained, by the Hartman's research group which started from a structure compatible with the hexagonal $P6_3/m$ space group.[7] As a matter of fact, by applying to the indexes of the faces the transformation matrix:

$$(h'k'l')_{\text{monoclinic}} = \begin{pmatrix} 0 & \bar{1} & 0 \\ 0 & 0 & 1 \\ \bar{2} & 0 & 0 \end{pmatrix} (hkl)_{\text{hexagonal}}$$

one obtains:

i) the set of the three monoclinic pinacoids {100}, {001}, {$\bar{1}$02} corresponds to the six faces of the hexagonal prism {10.0};

ii) the monoclinic pinacoid {010} corresponds to the hexagonal pinacoid {00.1};

iii) the set of the three monoclinic prisms {012}, {110} and {11$\bar{2}$} corresponds to the six faces of the hexagonal prism {01.1}.

These consideration are supported by the comparison of our results on the monoclinic HAp with those on the hexagonal one ($P6_3$) recently obtained[13] by the Ugliengo's group; this comparison is consistent for the reasons exposed in section 2 "Computational Details". Labeling with an apex the surface energy values of the hexagonal polymorph, one gets (in erg cm^{-2}): $\gamma'_{00.1}$= 1043, $\gamma'_{01.0}$= 1709, $\gamma'_{10.1}$= 1646, which have to be compared, respectively, with the ones of the monoclinic phase (Table 1 and 2): γ_{010} = 1041; γ_{001} = 1515, 1525, 1546, 1712, 1723, 1725; γ_{012} = 1637. The difference between $\gamma'_{01.0}$= 1709 and our lower values of γ_{001} =

1515, 1525, 1546, is surely due to the fact that inthe work of Corno et al.[13] the first set of (PO_4, Ca, OH) termination of the $d_{01.0}$ slice has not been considered. Nevertheless, the agreement is surprising.

On these grounds we can assess that it is quite difficult distinguishing the equilibrium shape of the monoclinic HAp from that of the hexagonal one.

At variance with the just mentioned agreement, the calculated value of γ_{001} = 1337 erg cm^{-2} for the monoclinic HAp[13] does not agree with the corresponding one we obtained (γ_{010} = 1041erg cm^{-2}); however, no information on the termination of the slab of thickness d_{002} was given by the authors.

Surface energy values of the hexagonal polymorph ($P6_3/m$) calculated by other groups, should be mentioned as well:

i) Lee et al.[8] obtained $\gamma_{01.0}$ = 1296 erg cm^{-2}, which is decidedly lower than both the γ_{001} (this work) and $\gamma'_{01.0}$= 1709.[13]

ii) Filgueiras et al.[10] predicted the ES by calculating the surface energy values for two surface profiles of each of the forms {00.1}, {11.1} and for six of the profiles of each of the forms {01.0}, {10.1} and {10.3}. The related ES is very different with respect to that shown in the present work, since the hexagonal bi-pyramid {10.1} is by far the most important form, and the pinacoid {00.1} does not enter the ES.

In our opinion, the results shown by Lee et al.[8] and Filgueiras et al.[10] could be handled with care since the empirical potentials adopted in both cases are not completely reliable.

b) Twinning of the monoclinic HAp reinforces the tendency of the monoclinic polymorph to mimic the hexagonal symmetry. It is worth remembering here, even if twinning cannot be considered an expression of the equilibrium, that one has to take into account the original composition planes for twinning should be parallel to flat (F) faces, in the sense of Hartman-Perdok. Having assumed as a twin axis a threefold one coincident with the diad axis of the single monoclinic crystal ($A_3 \equiv 2_1$),[18] three alternatives can be considered for the composition planes between parent (P) and twinned (T) individuals: $\{100\}_P \equiv \{001\}_T$, $\{100\}_P \equiv \{\bar{1}02\}_T$, $\{001\}_P \equiv \{\bar{1}02\}_T$. In a forthcoming paper we will show that the twin energy is very low and that, whatever the choice of the original composition plane for twinning, the morphology of simple and triple twins does progressively shift towards the hexagonal symmetry.

c) A final consideration is deserved to the implications of the relative stability of the faces (Fig. 7) on the HAp growth shape. Let's assume that the three pinacoids {100}, {001} and $\{\bar{1}02\}$, along with the {010} one, can grow by 2D nucleation, coherently with their F character. Remembering that: i) the activation energy for 2D nucleation (ΔG^*_{2D}) behaves like the square

of the sum of the specific energies (ρ_i) of the i - edges limiting the 2D nuclei : ≈ ^{2},

ii) it is reasonable assume that the edge energy ρ_i (erg cm^{-1}) is related to the surface energy γ_i (erg cm^{-2}) as $\rho_i = \gamma_i \times h_i$, where h_i is the height of the elementary i - step limiting the 2D nucleus, one can compare the activation energy for 2D-nucleation on {001} and {010} monoclinic forms:

a) for a rectangular nucleus forming on the {001} form: (001) ≈ (+ +2)×d_{002}

b) for a pseudo-hexagonal nucleus on the {010} form: (010) ≈ ( )×d_{020}

From Table 1 and from the thickness d_{002} and d_{020}, one obtains:

(010) / (001) = 0.58

This preliminary result means that the 2D nucleation frequency (J_{2D}) on the {010} form is surely favored with respect to the one on the faces belonging to the [010] zone, having kept in mind that the activation energy (scaled by k_BT) is the argument of the exponential term of the function:

$$J_{2D} \approx \exp(- / k_BT)$$

k_B being the Boltzmann's constant and T the absolute temperature.

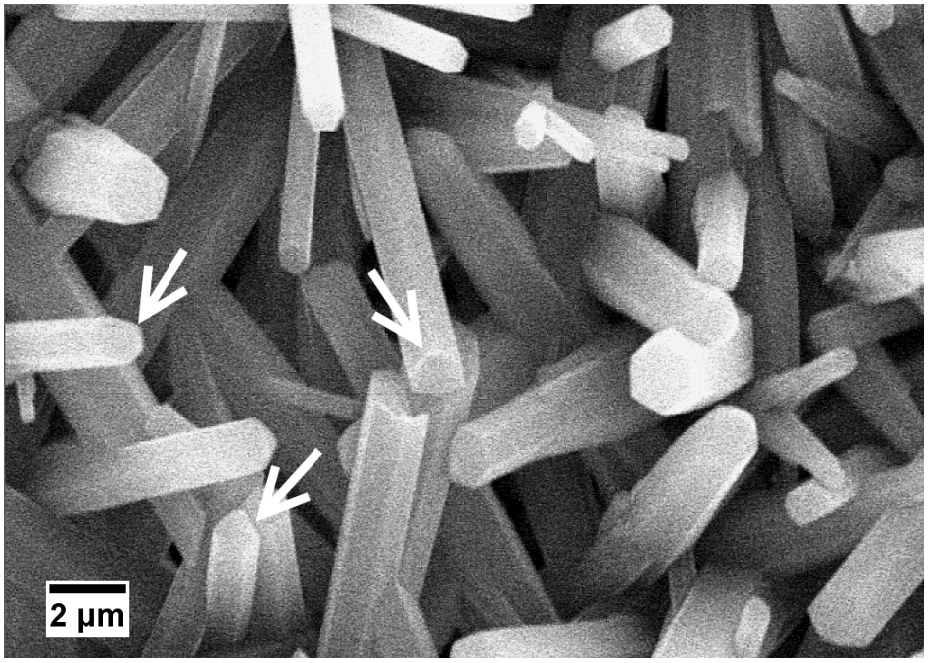

Figure 8. Growth morphology of monoclinic HAp crystals we obtained from cooling hot supersaturated aqueous solutions down to room temperature (for the experimental route, see Supporting Information). The shape of the basal faces (see arrows) perpendicular to the axes of the prismatic rods is pseudo-hexagonal.

Regardless of the adsorption effect of the solvent, we conclude that the privileged growth rate along the symmetry axis of both monoclinic and hexagonal HAp (Fig. 8) can be attributed, at first instance, to the anisotropic distribution of the edge energy in direction parallel and perpendicular to the symmetry twofold (or threefold) axis.

Acknowledgments

The study was financially supported by MIUR–Ministero dell'Istruzione, Università e Ricerca; MIUR-Project PRIN2010-2011, 2010EARRRZ_007: "Crystal-chemical and structural investigations on the bulk and surfaces of carbonated apatites with amorphous and nano-crystal transitions"

Supporting Information Available. Drawing of HAp structure: along the [010] direction with the slice of thickness $d_{10\bar{1}}$ (Figure S1); along the [100] direction with a possible configuration of the slice d_{020} (Figure S2); along the [100] direction with the four types of [100] PBC found: $[100]_A$, $[100]_B$, $[100]_C$ and $[100]_D$ (Figure S3); along the three main directions, [100], [001] and [201], all lying in the 010 plane and mutually rotated each other by near 120° (Figure S4). Computational details of the quantum-mechanical calculations performed on HAp. Experimental details for producing pure HAp from aqueous solution. This material is available free of charge via the Internet at http://pubs.acs.org.

References

(1) Posner, A.S.; Perloff, A.; Diorio, A.F. *Acta Cryst*. **1958**, *11*, 308.
(2) Kay, M.I.; Young, R.A.; Posner, A.S. *Nature* **1964**, *204*, 1050.
(3) Eysel, W.; Roy, D.M. *J. Cryst. Growth* **1973**, *20*, 245.
(4) Arends, J.; Shuthof, J.; van der Linden, W.H.; Bennema, P.; van den Berg, P.J. *J. Cryst. Growth* **1979**, *46*, 213.
(5) Mengeot, M.; Harvill, M.L.; Gilliam, O.R. *J. Cryst. Growth* **1973**, *19*, 199.
(6) Hughes, J.M.; Cameron, M.; Crowley, K.D. *Am. Miner.* **1989**, *74*, 870.

(7) Terpstra, R.A.; Bennema, P.; Hartman, P.; Woensdregt, C.F.; Perdok, W.G.; Senechal, M.L. *J. Cryst. Growth* **1986**, *78*, 468.
(8) Lee, W.T.; Dove, M.T.; Salje, E.K.H. *J. Phys: Condensed Matter* **2000,** *12*, 9829.
(9) De Leeuw, N.H. *Phys. Chem. Chem. Phys.* **2002**, *4*, 3865.
(10) Filgueiras, M.R.T.; Mkhonto, D.; de Leeuw, N.H. *J. Cryst. Growth* **2006**, *294*, 60.
(11) De Leeuw, N.H.; Rabone, J.A.L. *CrystEngComm.* **2007**, *9*, 1178.
(12) Matsunaga, K.; Murata, H. *Materials Transactions* **2009**, *50*, 1041.
(13) Corno, M.; Orlando, R.; Civalleri, B.; Ugliengo, P. *Eur. J. Mineral*. **2007**, *19*, 757.
(14) Corno, M.; Rimola, A.; Bolis, V.; Ugliengo, P. *Phys. Chem. Chem. Phys.* **2010**, *12*, 6309.
(15) Bolis, V.; Busco, C.; Martra, G.; Bertinetti, L.; Sakhno, Y.; Ugliengo, P.; Chiatti, F.; Corno, M.; Roveri, N. *Phil. Trans. Royal Soc.* **2012**, *A370*, 1313.
(16) Sudarsanan, K.; Young, R.A. *Acta Crystallogr. B. Struct. Crystallogr. Cryst. Chem.* **1969**, *25*, 534.
(17) Young R.A.; Elliot J.C. *Archs. Oral Biol.* **1966**, *11*, 699.
(18) Prener, J.S. *J. Electrochem. Soc*. **1967**, *114*, 77.
(19) Elliott, J.C. *Nature Phys. Sci.* **1971**, *230*, 72.
(20) Elliott, J.C. Young, R.A. *Nature* **1967**, *214*, 904.
(21) Elliott, J.C.; Mackie, P.E.; Young, R.A. *Science, New Series* **1973**, *180(4090)*, 1055.
(22) Ikoma, T.; Yamazaki, A.; Nakamura, S.; Akao, M. *J. Solid State Chemistry* **1999**, *144*, 272.
(23) Suetsugu, Y.; Tanaka, J. *J. Mat. Sci. Mater. in Medecine* **2002**, *13,* 767.
(24) Suda, H.; Yashima, M.; Kakihana, M.; Yoshimura, M. *J. Phys. Chem.* **1995**, *99*, 6752.
(25) Ikoma, T.; Yamazaki, A.; Nakamura, S.; Akao, M. *NetsuSokutei* **1998**, *25,* 141.
(26) Treboux, G.; Layrolle, P.; Kanzaki, N.; Onuma, K.; Ito, A. *J. Am. Chem. Soc.* **2000**, *122,* 8323.
(27) Hochrein, O.;Kniep, R.; Zahn, D. *Chem. Mater.* **2005,** *17***,** 1978.
(28) Haverty, D.; Tofail, S.A.M.; Stanton, K.T.; Mc Monagle, J.B. *Phys. Rev. B* **2005**, *71*, 094103.
(29) Corno, M.; Busco, C.; Civalleri, B.; Ugliengo, P. *Phys. Chem. Chem. Phys.* **2006**, *8*, 2464.
(30) Ma, G.; Liu, X.Y. *Cryst. Growth Des*. **2009**, *9*, 2991.
(31) Hartman, P.; Perdok, W.G. *Acta Cryst.* **1955**, *8*, 521.
(32) Kern, R. The Equilibrium Form of a Crystal, in Morphology of crystals, Ed. I. Sunagawa, Reidel Publ. (1987) p. 77–206.
(33) Dovesi, R.; Civalleri, B.; Orlando, R.; Roetti, C.; Saunders, V.R. In: Reviews in Computational Chemistry; Lipkowitz, B.K.; Larter, R.; Cundari, T.R., Eds.; John Wiley & Sons, Inc.: New York, 2005, vol.1, p.443.
(34) Dovesi, R.; Orlando, R.; Civalleri, B.; Roetti, C.; Saunders, V.R.; Zicovich-Wilson, C.M. *Z. Kristallogr.* **2005**, *220*, 571.
(35) Dovesi, R. *et al.*, *CRYSTAL09 User's Manual*; University of Torino: Torino, Italy, 2009.
(36) Pisani, C.; Dovesi, R.; Roetti, C. *Hartree-Fock ab-initio treatment of crystalline systems*, Lecture Notes in Chemistry; Springer: Berlin, Heidelberg, New York, 1988.
(37) Becke, A.D. *J. Chem. Phys.* **1993**, *98*, 5648.
(38) Lee, C.; Yang, W.; Parr, R.G. *Phys. Rev. B* **1998**, *37*, 785.
(39) Stephens, P.J.; Devlin, F.J.; Chabalowski, C.F.; Frisch, M.J. *J. Phys. Chem.* **1994**, *98*, 11623.

For Table of Contents Use Only

The Low Symmetry Polymorph of Hydroxyapatite. Theoretical Equilibrium Morphology of the Monoclinic $Ca_5(OH)(PO_4)_3$

Dino Aquilano,[1] Marco Bruno,[1] Marco Rubbo,[1] Francesco Roberto Massaro,[2] Linda Pastero[1]

[1]*Dipartimento di Scienze della Terra, Università degli Studi di Torino, via Valperga Caluso 35, I-10125, Torino, Italy*

[2]*Dipartimento di Geoscienze, Università degli Studi di Padova, Via Gradenigo 6, I-35131, Padova, Italy*

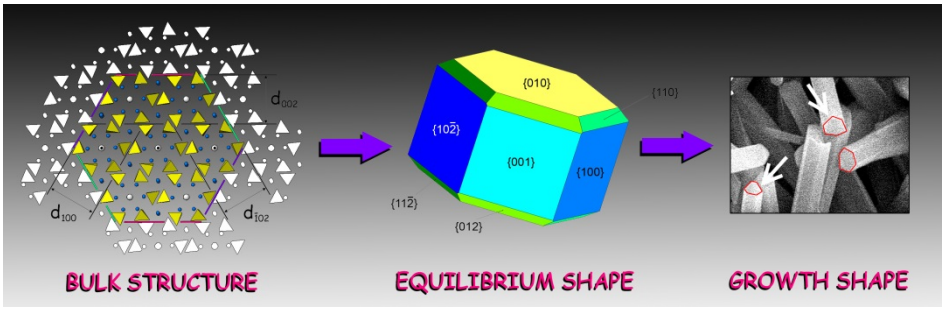

Synopsis

The theoretical equilibrium shape of the monoclinic Hydroxyapatite (HAp) is derived from coupling the Hartman-Perdok analysis of the HAp bulk structure with the *ab initio* calculation of the different {hkl} surface energies. The growth shape, consisting of rod crystals truncated by the pseudo-hexagonal {010} form, is derived by a qualitative kinetic model.